Journal of Nuclear and Radiochemical Sciences, Vol. 5, No. 2, pp. 27-31, 2004

Theoretical Analysis of Electronic Structure for the Chemical Bonding of Pu and Am in MgO

Kumiko Tanaka,*[,a,b] Masaru Hirata,[b] and Rika Sekine[a]

[a]*Department of Chemistry, Faculty of Science, Shizuoka University, 836 Ohya, Shizuoka 422-8529, Japan*
[b]*Department of Materials Science, Japan Atomic Energy Research Institute, Tokai-mura, Naka-gun, Ibaraki 319-1195, Japan*

Received: September 8, 2004; In Final Form: October 18, 2004

The relativistic discrete-variational Dirac-Fock-Slater (DV-DFS) method was performed to investigate the electronic structure of MgO doped with Pu or Am atoms. The differences between these systems, in particular, the participation of *d*-electrons and *f*-electrons in chemical bonding, were clarified by calculating their electronic structures. Substitution of actinide atoms was found to result in the effective charges of MgO becoming smaller, with a large charge transfer occurring as far as the second layer. It was also found that the bonding feature between the center atom and the surrounding oxygen atoms was extended to lower energy in the case of actinide (An) substituted systems. Moreover, the bonding characteristics were assigned; a bonding interaction for An*6d*-O2*p* and an anti-bonding for An*5f*-O2*p* near the HOMO level. These complex effects were found to dominate the strength of the covalent bonding between MgO and actinide atoms.

1. Introduction

The electronic structures of metal oxides containing actinide atoms give essential information on the interaction between the actinide atoms and base metal oxides. In the field of nuclear technology and science, magnesium oxide,[1–4] zirconium oxide,[4, 5] and spinel[6, 7] are appropriate candidates for an inert matrix, which acts as a mechanical support and diluent, used in transmutation of actinides (An), such as plutonium (Pu) and americium (Am).[8] Early study[9] indicated that magnesium oxide (MgO) was considered to be the most appropriate support material for transmutation of Am because of its desirable properties, such as high melting point, relatively high thermal conductivity and high mobility of helium.[10] Researches of the thermophyisical properties of doped actinides in metal oxides are accumulated so far, however less work has focused on the electronic structures and chemical bonding nature of these systems to understand the physical and chemical properties.

The electronic configurations of the actinides also provide insight into the properties of their compounds. The difference between the electronic configuration of neutral Pu and Am atoms is only one *f*-electron (Pu: $5f^6 6d^0 7s^2 7p^0$, Am: $5f^7 6d^0 7s^2 7p^0$); however, the *f*-electrons of lighter actinides (Pa–Pu) are considered to have an itinerant trend,[11, 12] on the other hand, the *f*-electrons of transplutonium elements (Am–Cf) have localized character and behave more like the lanthanides. It is known that a boundary of the chemical and physical properties lies between Pu and Am.[13] For example, Np and Pu metals have the unique properties; such as low-symmetry of crystal structure (monoclinic) at room temperature, low melting point, and multiple phase transition. On the other hand, transplutonium metals have more symmetric hexagonal close-packed structure and relatively higher melting point than Np and Pu. Furthermore, a large variation in stoichiometry is found in the actinide oxides. The sesquioxide becomes the predominate oxide for the transplutonium elements, in contrast to the lighter actinides prefer to have higher valence.

The present study is undertaken with the goal of advancing our understanding of fundamental chemical bonding between actinide atom and metal oxides. The relativistic discrete-variational Dirac-Fock-Slater (DV-DFS) method was applied to investigate the electronic structure of MgO doped with Pu or Am atoms. This method gives reliable information of chemical bonding even for heavy system such as the actinide series. Although there are several theoretical studies of pure actinide oxides,[14–18] the interaction between actinide atoms and an inert matrix has not been well clarified until now. The current investigation focused on the difference between these systems, in particular, the participation of *d*-electrons and *f*-electrons in the chemical bonding.

2. Computational Method

The DV-DFS molecular orbital (MO) method, based on the Dirac-Fock-Slater (DFS) approximation, was used to perform cluster calculations of pure MgO and actinide doped MgO. This method provides a powerful tool for the study of the electronic structure of molecules and solids containing heavy elements.[14, 16, 19–23] The detailed procedure has been published elsewhere.[24–26]

The schematic representation of a model cluster of MgO is shown in Figure 1. MgO has NaCl structure and all bond length

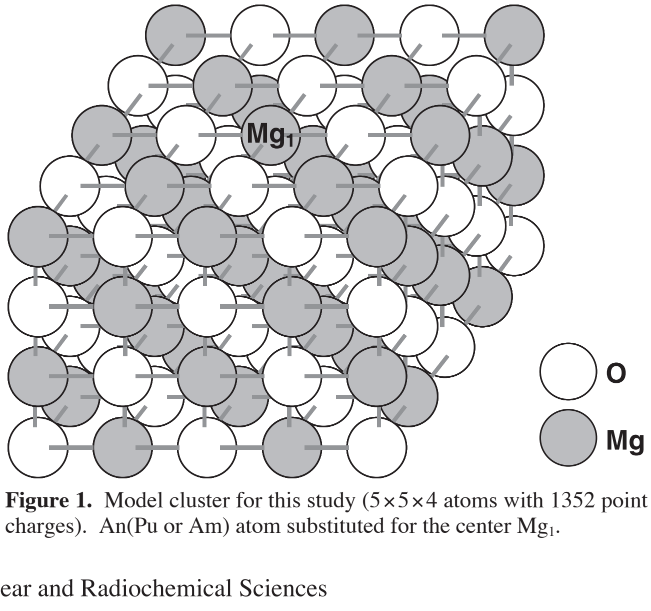

Figure 1. Model cluster for this study (5×5×4 atoms with 1352 point charges). An(Pu or Am) atom substituted for the center Mg_1.

---

*Corresponding author. E-mail: kumi-tnk@popx.tokai.jaeri.go.jp. FAX: +81-29-282-6723.

© 2004 The Japan Society of Nuclear and Radiochemical Sciences
Published on Web 11/11/2004

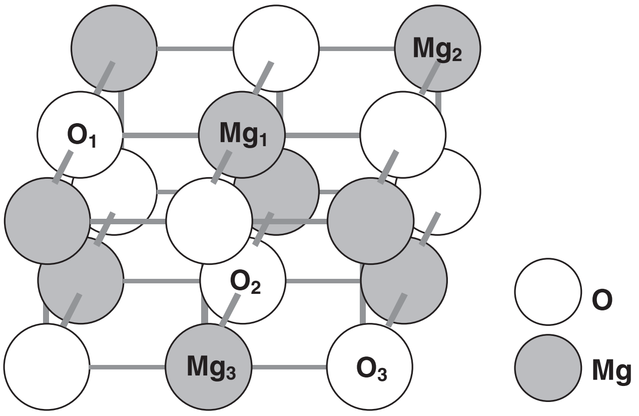

Figure 2. Magnification of a part of model cluster. The center Mg$_1$ was substituted by Pu or Am atom.

between Mg and O is fixed to 210.6 pm. The calculation, when performed for insulators such as magnesium oxides, is difficult because of the long-range Coulomb interactions even from distant atoms. In order to represent the effect, 1352 points of +2 and –2 point charges (PC) were placed at the lattice positions around the cluster model. These PC guaranteed that the Madelung potential inside the cluster was properly reproduced. Figure 2 shows a part of the model cluster, cutting away the substituted center atom and surrounding atoms from Figure 1. The Pu or Am doped MgO system was also calculated, using the model cluster with substitution of an An atom for the center Mg$_1$ atom as shown in Figure 2. For the initial charge, An atoms were assigned as trivalent and the other atoms as divalent, in other words, the electronic configurations were Pu: $5f^5 6d^0 7s^0 7p^0$, Am: $5f^6 6d^0 7s^0 7p^0$, Mg: $2s^2 2p^6 3s^0 3p^0$, and O: $2s^2 2p^6 3s^0 3p^0$. The bond length of Pu-O$_2$ and Am-O$_2$ were estimated from the ionic radius of the trivalent atom, and were determined to be 238.39 pm and 235.91pm, respectively. The lattice relaxation caused by An substitution was not considered in the present calculation, therefore, only the bond lengths between metals (Mg$_1$, Pu, or Am) and adjacent oxygens (O$_1$, O$_2$) were changed.

3. Results and Discussion

3.1. Effective Charge and Ionic Interaction. Table 1 shows the effective charges on substituted Pu (Pu+MgO), Am (Am+MgO) and the surrounding Mg and O with reference to the pure MgO (Mg+MgO). The positions of these atoms are indicated in Figure 2. The Mulliken population analysis[27] is known to have a basis set dependence; however, the analysis provides qualitative aspects of the chemical bonding. In this calculation, numerical basis sets[28] were generated for Pu, Am, Mg, and O atoms, with the same conditions, so that the effect of the basis set on the orbital population was negligible. As shown in Table 1, the effective charges of Mg and O became fairly small in consequence of the An substitution, and a large charge transfer to the second layer occurred. Plutonium has a slightly larger effective charge (0.53) than Am (0.50) and this indicates that Pu prefers to have a higher oxidation state than Am. It is known that MgO is a strongly ionic system, and therefore the HOMO-LUMO gap of Mg+MgO is calculated as 4.18 eV; however, that of the Pu+MgO (0.55 eV) and Am+MgO (0.02 eV) systems were found to be small in this study. This indicates that the ionic bonding strength becomes weak and the systems become unstable as a result of An substitution.

TABLE 1: Effective Charge of Center Atom (Mg$_1$, Pu, or Am) and Neighbor Mg and O

	Mg+MgO	Pu+MgO	Am+MgO
Mg(An)$_1$	0.71	0.53	0.50
Mg$_2$	0.72	0.37	0.38
Mg$_3$	0.64	0.28	0.29
O$_1$	-0.74	-0.21	-0.23
O$_2$	-0.70	-0.25	-0.26
O$_3$	-0.72	-0.37	-0.38

Table 2 shows the occupation number of the valence orbitals for the Mg+MgO, Pu+MgO, and Am+MgO systems. When comparing the final orbital occupations with the initial ones, the number of electrons of Mg*3s*, Mg*3p*, An*6d*, An*7s*, and An*7p* orbitals increase and only that of the *5f* orbital slightly decrease. A significant change in the orbital population was observed in the increase of the *6d* electron for the An+MgO system. The Pu*6d* orbital receives 1.84 electrons from the surrounding oxygen atoms, while the Am*6d* orbital receives 1.79 electrons. It follows from these results that the number of electrons in the *5f* orbital is directly proportional to the atomic number, but that of the *6d* orbital is inversely proportional in the MgO environment. The occupation numbers of O2*s* and O2*p* become smaller with An substitution. The O$_1$*2s*, O$_1$*2p*, O$_2$*2s*, and O$_2$*2p* orbitals release 0.07, 0.47, 0.05, and 0.40 electrons, respectively, in the Pu+MgO system, and 0.06, 0.46, 0.05, and 0.40, respectively, in the Am+MgO system. This indicates that charge transfer occurs mainly from the O2*p* oribtal to An*6d* orbital. The occupation of the Pu*6d* orbital is larger than that of Am*6d*, however, the total charge transfer between Am and the surrounding oxygen (+2.50), and also that for Pu (+2.46).

3.2. Analysis of Covalent Bonding. In order to evaluate covalent interactions between substituted Pu, Am, and the surrounding oxygens, bond overlap population (BOP) analyses were obtained, as shown in Table 3. After substitution of An for Mg, the interaction between the An atom and the surrounding oxygen (O$_1$, O$_2$) becomes larger than that for Mg. The BOP for Pu+MgO is slightly larger than Am+MgO. On the other hand, the bonding of Mg$_2$-O$_1$, Mg$_3$-O$_1$, and Mg$_3$-O$_2$ becomes weak, because electrons move to the surrounding of An and a strong interaction between An and oxygen is generated by An substitution.

TABLE 2: Orbital Occupations of Valence Orbitals

Mg+MgO			Pu+MgO	Am+MgO
		An $5f_{5/2}$	3.90	4.74
		An $5f_{7/2}$	0.95	1.16
		An $6d_{3/2}$	0.77	0.75
		An $6d_{5/2}$	1.07	1.04
Mg$_1$ $3s$	0.48	An $7s$	0.39	0.40
Mg$_1$ $3p_{1/2}$	0.27	An $7p_{1/2}$	0.22	0.23
Mg$_1$ $3p_{3/2}$	0.54	An $7p_{3/2}$	0.20	0.21
O$_1$ $2s$	1.80	O$_1$ $2s$	1.73	1.74
O$_1$ $2p_{1/2}$	1.65	O$_1$ $2p_{1/2}$	1.50	1.50
O$_1$ $2p_{3/2}$	3.29	O$_1$ $2p_{3/2}$	2.97	2.98
O$_2$ $2s$	1.78	O$_2$ $2s$	1.73	1.73
O$_2$ $2p_{1/2}$	1.64	O$_2$ $2p_{1/2}$	1.51	1.51
O$_2$ $2p_{3/2}$	3.28	O$_2$ $2p_{3/2}$	3.01	3.01

TABLE 3: Bond Overlap Population between Center Atom (Mg$_1$, Pu, or Am) and Neighbor Oxygen (O$_1$, O$_2$)

	Mg+MgO		Pu+MgO		Am+MgO	
	O$_1$	O$_2$	O$_1$	O$_2$	O$_1$	O$_2$
Mg(An)$_1$	0.32	0.26	0.55	0.39	0.54	0.38
Mg$_2$	0.65	-0.20	0.46	-0.10	0.47	-0.10
Mg$_3$	0.24	1.23	0.18	1.03	0.20	1.04

TABLE 4: Orbital Overlap Population between Valence Orbital of Center Atom (Mg_1, Pu, or Am) and O_1 and O_2

Mg+MgO					Pu+MgO					Am+MgO			
	O_1 *2s*	O_1 *2p*	O_2 *2s*	O_2 *2p*		O_1 *2s*	O_1 *2p*	O_2 *2s*	O_2 *2p*	O_1 *2s*	O_1 *2p*	O_2 *2s*	O_2 *2p*
					An *5f*	0.01	0.10	0.00	0.02	0.01	0.08	0.00	0.01
					An *6d*	0.05	0.28	0.01	0.09	0.05	0.27	0.01	0.09
Mg_1 *3s*	-0.01	0.12	0.00	0.06	An *7s*	0.01	0.07	0.01	0.05	0.01	0.07	0.01	0.05
Mg_1 *3p*	0.07	0.16	0.01	0.06	An *7p*	0.10	0.07	0.01	0.03	0.11	0.07	0.01	0.03

The analysis of orbital contributions to the chemical bonding is useful to understand the nature of *6d* and *5f* electrons in the actinide systems. Table 4 provides the orbital overlap populations between the valence orbitals of An-O_1 and An-O_2. The main difference between the Pu+MgO and Am+MgO systems are the An*5f*-O*2p* and An*6d*-O*2p* orbital overlap populations. Both of the orbital overlap populations for Pu*5f*-O*2p* and Pu*6d*-O*2p* are larger than those for Am*5f*-O*2p* and Am*6d*-O*2p*. This causes a larger interaction between Pu and O_1, than that for Am; however such a discrepancy is obscure in the case of An and O_2. As indicated in Table 2, the number of *6d* electrons directly influences the An*6d*-O*2p* orbital overlap population, however the influence of *5f* occupation reveals an opposite trend. In order to sufficiently examine the contribution of *6d* and *5f* orbitals toward chemical bonding, the participation of the valence orbitals was analyzed for bonding features.

Figure 3 illustrates the bonding features of the central Mg atom with neighboring O_1 or O_2 for the Mg+MgO system versus the molecular orbital (MO) energy. The figures consist of the calculated partial density of states (PDOS) for O*2p*, Mg*3s*, and Mg*3p*, which are main components of the valence band, together with the BOP between Mg and O_1 or O_2. Vertical lines shown in the figures of PDOS are the energy levels of each component. In these figures, the HOMO level, was calibrated to be 0 eV, and positive and negative values of the BOP signify bonding and anti-bonding features, respectively, for the corresponding MO. The valence band of Mg+MgO contains mainly an O*2p* component plus some components of Mg*3p* and Mg*3s*, implying that Mg+MgO is a strongly ionic system. From these figures, the bonding features show a similar trend to the PDOS for the O*2p* orbital in both the Mg-O_1 and Mg-O_2 cases. Moreover, the strengths of covalent bonding for Mg-O_1 and Mg-O_2 are almost the same, although the dominant bonding features appear at different energy levels.

The principal features of BOP and PDOS of corresponding energy are indicated as arrows and categorize into five parts. The small Mg*3p* orbital is distributed from the HOMO to about –1.5 eV, and has bonding interaction (**b**) with the O*2p* orbital, while anti-bonding interaction indicated as feature (**a**) is predominant around the HOMO level. The Mg*3s* orbital appears from about –1.5 eV, and has bonding interaction (**c**) with the O*2p* orbital in Mg-O_1 and in Mg-O_2. The Mg*3p* and the Mg*3s* orbitals are hybridized from about –2.5 to –3.5 eV, and have bonding interaction (**d**) with the O*2p* orbital. The Mg*3p* and the Mg*3s* orbitals appear again from approximately –3.5 eV and –5.0 eV, respectively, and have bonding interaction (**e**) with the O*2p* orbital. It is noted that almost all interactions of O*2p*-Mg*3s*, O*2p*-Mg*3p*, and O*2p*-Mg*3s*-Mg*3p* indicate bonding features, but the MO close to the HOMO level shows anti-bonding features, which appear clearly in the bonding of Mg-O_2, than that of Mg-O_1.

The valence band of the Pu+MgO system mainly contains an O*2p* component plus some Pu*5f* and Pu*6d* components. The PDOS of O*2p*, Pu*5f*, and Pu*6d* together with the BOP between Pu and O_1 or O_2 are illustrated in Figure 4. From these figures, it can be presumed that almost all bonding features mainly consist of Pu*6d*-O*2p* interactions. The O_1*2p* and O_2*2p* orbitals appear around 3.0 eV deeper in energy than the case of Mg+MgO, with the shift caused by the charge transfer between Pu and oxygen. The covalent bonding of Pu-O_1 becomes stronger than that of Pu-O_2, and consequently, the reinforcement of lateral bonding arises from Pu substitution for Mg. The orbital interaction can be approximately divided into three parts, as shown in these figures. The large components of Pu*5f* are distributed around the HOMO, and have anti-bonding interaction (**a**) with the O*2p* orbital in Pu-O_2. The Pu*5f* and Pu*6d* orbitals are distributed from about –0.5 to –6.5 eV, and interact with the O*2p* orbital in both bonding and anti-bonding characteristics (**b**). The Pu*5f*, Pu*6d*, and O*2p* orbitals are well hybridized and the largest BOP in Pu-O_2 is due to this hybridization. The Pu*6d* orbital is also distributed from about –6.5 to –8.0 eV, and interacts with the O*2p* orbital as large bonding features (**c**), as shown in Figure 4. The overlap of the O*2p* and Pu*6d* orbitals becomes large, because of the shift of O*2p* orbitals toward

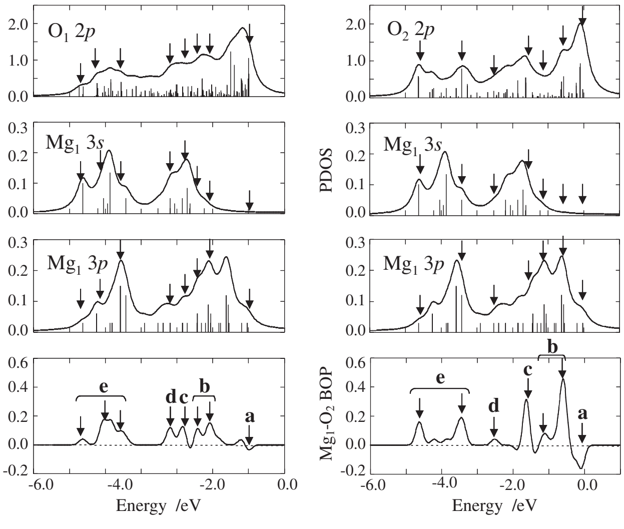

Figure 3. Bond overlap population of Mg_1-O_1 and Mg_1-O_2.
a, **b**: Mg*3p*-O*2p* interaction, **c**: Mg*3s*-O*2p* interaction, **d**: Mg*3s*-Mg*3p*-O*2p* hybridization and **e**: Mg*3p*-O*2p* and Mg*3p*-O*2p* interaction

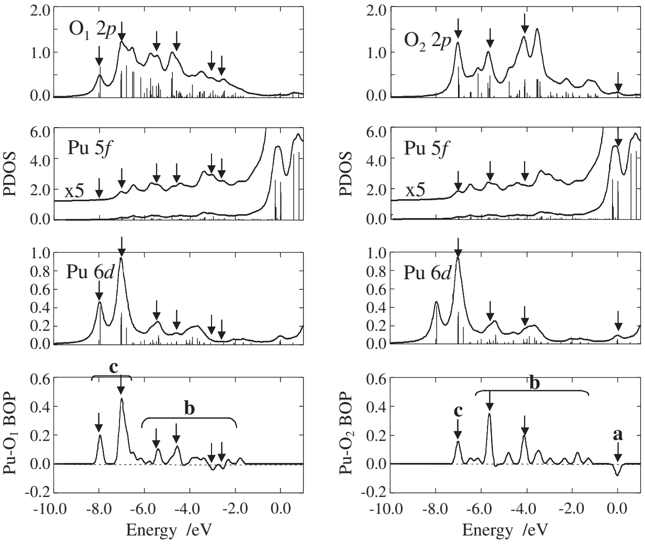

Figure 4. Bond overlap population of Pu-O_1 and Pu-O_2.
a: Pu*5f*-O*2p* interaction, **b**: Pu*5f*-Pu*6d*-O*2p* hybridization and **c**: Pu*6d*-O*2p* interaction

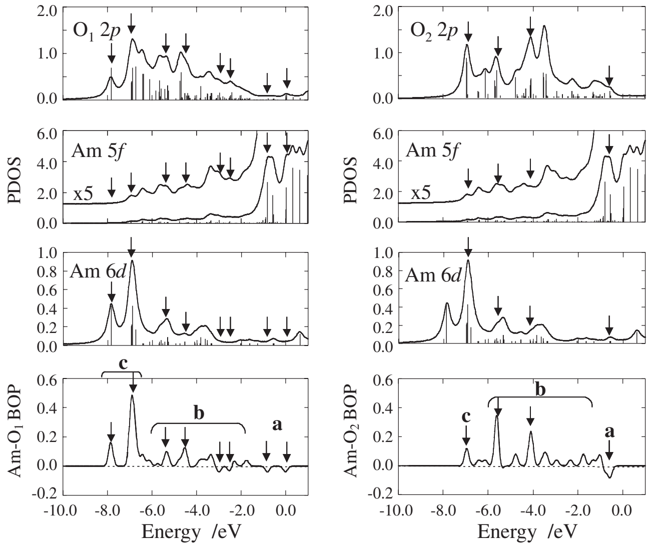

Figure 5. Bond overlap population of Am-O_1 and Am-O_2.
a: Am*5f*-O*2p* interaction, **b**: Am*5f*-Am*6d*-O*2p* hybridization and **c**: Am*6d*-O*2p* interaction

lower energy, which was caused by the charge transfer between Pu and oxygen, and consequently, a largest bonding feature arises. From these results, it has been clarified that O*2p*-Pu*6d* interaction plays an important role for the bonding of Pu-O_1 and Pu-O_2.

The PDOS of O*2p*, Am*5f*, and Am*6d*, for the Am+MgO system, together with the BOP between Am and O_1 or O_2, are shown in Figure 5. The valence band of the Am+MgO system, like Pu+MgO, mainly contains an O*2p* component plus some Am*5f* and Am*6d* components, and the general trends are nearly similar to the Pu+MgO system. In order to analyze the discrepancy between these two systems, the principal features of BOP and PDOS of corresponding energy were indicated as arrows for the Am+MgO. The orbital interaction can be divided into three parts. The large components of the Am*5f* orbital are distributed from the HOMO to –1.0 eV, and have anti-bonding interaction (**a**) with the O*2p* orbital. The Am*5f* and Am*6d* orbitals are distributed from –1.0 to –6.5 eV, and interact toward the O*2p* orbital with both bonding and anti-bonding characteristics (**b**). The Am*5f*, Am*6d*, and O*2p* orbitals are well hybridized, however these hybridized MOs are fewer than those of the Pu system. The hybridization also produces the largest bonding feature in Am-O_2, while it contributes a small anti-bonding feature in Am-O_1. The Am*6d* orbital is distributed from –6.55 to –8.0 eV, and has bonding interaction (**c**) with the O*2p* orbital. The intensity of the O*2p*-Am*6d* interaction is similar to that of O*2p*-Pu*6d*, however the orbital occupation of Am*6d* is less than that of Pu*6d*, as shown in Table 2. That is, Am-O_1 and Am-O_2 interactions are weaker than those of Pu-O_1 and Pu-O_2. The most important difference between the Pu+MgO and Am+MgO systems is the electronic structures around the Fermi energy, which are assigned to O*2p*-An*5f* interaction. Apparently, the overlap of Am*5f*-O*2p* is larger than that for Pu, in proportion to the orbital occupation of An*5f*, but this interaction has anti-bonding characteristic, and therefore the chemical bonding for Am-O_1 and Am-O_2 is weaker than that for Pu-O_1 and Pu-O_2.

Consideration of the charge density of an ideally isolated ion is subtracted from that of the cluster (the difference in charge density) of the interatomic region can provide additional insight into clarifying the covalent bonding in these systems.[29] The difference in charge densities of Pu-O_1 and Am-O_1 are shown in Figure 6, compared with those of Mg_1-O_1. The Mg, Pu, and Am atomic positions are at $r = 0.0$ pm, and O_1 is at $r = 210.6$ pm. From the difference in charge density of Mg_1-O_1, no electrons binding two nuclei are exhibited to generate covalent bonding.

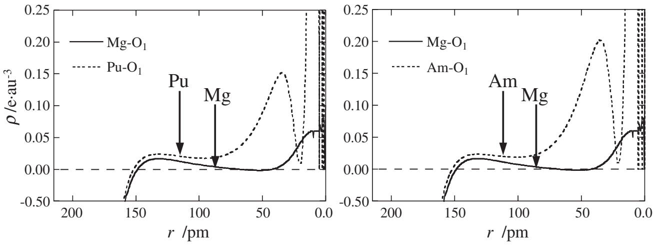

Figure 6. Cross sectional view of the difference in charge density for Pu-O_1 and Am-O_1 comparing with Mg_1-O_1. Atomic unit (au) is Bohr radius, which corresponds to 52.9 pm.

On the other hand, the charge densities for the Pu-O_1 and Am-O_1 bonds increase in the interatomic region. The difference in the charge densities of Mg, Pu, and Am are 0.004, 0.021 and 0.020 at the ionic radius of the metal atom (Pu(III) = 114.0 pm, Am(III) = 111.5 pm, Mg(II) = 86.0 pm),[30] respectively. This indicates that ionic bonding dominates the chemical bonding of Mg_1-O_1, and covalent bonding dominates in the chemical bonding of An-O_1. In the case of An-O_1, increases of the difference in charge density inside the An atoms are appreciable. The increase implies that the An*5f* electron participates in shielding the nuclear charge, which makes the effective charge of the An atom small. Moreover, a remarkable discrepancy between the bonding nature of Pu-O_1 and Am-O_1 is recognized in this shielding.

4. Conclusions

In order to investigate the electronic structure of MgO doped with Pu or Am atoms, the relativistic discrete-variational Dirac-Fock-Slater (DV-DFS) method was performed. It was found that the effective charges of Mg and O become small, in consequence of the An substitution, in addition to a large charge transfer that reached to the second layer. Furthermore, the effective charge of Pu (0.53) and Am (0.50) indicated that Pu prefers to have a higher oxidation state than Am. Using a combination of PDOS for the main components of the valence band of the Mg+MgO, Pu+MgO, and Am+MgO systems, and the BOP between the Metal (Mg, Pu, or Am)-O_1 and Metal-O_2 versus the MO energy, the contribution of these atomic orbitals to the chemical bonding was clarified. In the case of the Mg+MgO system, almost all interactions for O*2p*-Mg*3s*, O*2p*-Mg*3p*, and O*2p*-Mg*3s*-Mg*3p* exhibited bonding features, although those for O*2p*-Mg*3p* near the HOMO level showed anti-bonding features. Conversely, in the case of the An+MgO system, the largest bonding feature is produced from interactions of An*6d*-O*2p*, and the reinforcement of lateral bonding occurred by an An substitution for Mg. One of the essential results of this calculation is the interpretation of the chemical bonding nature of An doped MgO. The interaction of An*6d*-O*2p* plays an important role, however, that of An*5f*-O*2p* is also effective for determining the bonding strength between An and the surrounding oxygens, because of their anti-bonding feature. Furthermore, it was revealed that the strength of both the ionic and covalent bonding are stronger in the Pu+MgO system than the Am+MgO system, and these results implied that the stability of Pu in MgO is higher than Am in MgO. The difference in the charge density of An-O_1 exhibited an increase in density inside the An atoms, which implied a contribution of the An*5f* electron in screening the charges. In the present study, the participation of *d*- and *f*-electrons in chemical bonding was evaluated, and the results suggest that charge screening occurred due to An*5f* electrons.

References

(1) K. Bakker and R. J. M. Konings, J. Nucl. Mater. **254**, 129 (1998).

(2) K. Bakker and R. J. M. Konings, J. Nucl. Mater. **271-273**, 632 (1998).
(3) C. Ronchi, J. P. Ottaviani, C. Degueldre, and R. Calabrese, J. Nucl. Mater. **320**, 54 (2003).
(4) Y. Croixmarie, E. Abonneau, A. Fernández, R. J. M. Konings, F. Desmoulière, and L. Donnet, J. Nucl. Mater. **320**, 11 (2003).
(5) P. E. Raison and R. G. Haire, J. Nucl. Mater. **320**, 31 (2003).
(6) R. J. M. Konings, R. Conrad, G. Dassel, B. J. Pijlgroms, J. Somers, and E. Toscano, J. Nucl. Mater. **282**, 159 (2000).
(7) T. Wiss, R. J. M. Konings, C. T. Walker, and H. Thiele, J. Nucl. Mater. **320**, 85 (2003).
(8) M. Burgharts, Hj. Matzke, C. Léger, G. Vambenepe, and M. Rome, J. Alloy. Comp. **271-273**, 544 (1998).
(9) N. Chauvin, R. J. M. Konings, and Hj. Matzke, J. Nucl. Mater. **274**, 105 (1999).
(10) A. van Veen, R. J. M. Konings, and A. V. Fedorov, J. Nucl. Mater. **320**, 77 (2003).
(11) Q. G. Sheng, B. R. Cooper, and S. P. Lim, J. Appl. Phys. **73**, 5409 (1993).
(12) D. van der Marel and G. A. Sawatzky, Phys. Rev. B **37**, 10674 (1988).
(13) R. G. Haire, J. Alloy. Comp. **223**, 185 (1995).
(14) V. A. Gubanov, A. Rosén, and D. E. Ellis, J. Phys. Chem. Solids. **40**, 17 (1979).
(15) G. L. Goodman, J. Alloy. Comp. **181**, 33 (1992).
(16) S. Xia and J. C. Krupa, J. Alloy. Comp. **307**, 61 (2000).
(17) K. N. Kudin, G. E. Scuseria, and R. L. Martin, Phys. Rev. Lett. **89**, 266402 (2002).
(18) L. Petit, A. Svane, Z. Szotek, and W. M. Temmerman, Science **301**, 498 (2003).
(19) M. Hirata, H. Monjyushiro, R. Sekine, J. Onoe, H. Nakamatsu, T. Mukoyama, H. Adachi, and K. Takeuchi, J. Electron Spectrosc. Relat. Phenom. **83**, 59 (1997).
(20) J. Onoe, K. Takeuchi, H. Nakamatsu, T. Mukoyama, R. Sekine, and H. Adachi, J. Electron Spectrosc. Relat. Phenom. **70**, 89 (1992).
(21) M. Kurihara, M. Hirata, R. Sekine, J. Onoe, H. Nakamatsu, T. Mukoyama, and H. Adachi, J. Alloys Compd. **283**, 128 (1999).
(22) M. Kurihara, M. Hirata, R. Sekine, J. Onoe, and H. Nakamatsu, J. Nucl. Mater. **281**, 140 (2000).
(23) M. Kurihara, M. Hirata, R. Sekine, J. Onoe, and H. Nakamatsu, J. Nucl. Mater. **326**, 75 (2004).
(24) A. Rosen and D. E. Ellis, J. Chem. Phys. **62**, 3039 (1975).
(25) H. Adachi, A. Rosen, and D. E. Ellis, Mol. Phys. **33**, 199 (1977).
(26) H. Nakamatsu, H. Adachi, and T. Mukoyama, Bull. Inst. Chem. Res. Kyoto Univ. **68**, 304 (1991).
(27) R. S. Mulliken, J. Chem. Phys. **23**, 1841 (1955).
(28) H. Adachi, M. Tsukada, and C. Satoko, J. Phys. Soc. Jpn. **45**, 875 (1978).
(29) H. Nakamatsu, T. Mukoyama, and H. Adachi, Chem. Phys. Lett. **247**, 168 (1995).
(30) R. D. Shannon, Acta Cryst. **A32**, 751 (1976).